JOURNAL OF COMPUTATIONAL PHYSICS 37, 93–112 (1980)

Spectral Methods for Multi-dimensional Diffusion Problems

ROBERT L. MCCRORY

Laboratory for Laser Energetics, University of Rochester
Rochester, New York 14627

AND

STEVEN A. ORSZAG

Department of Mathematics, Massachusetts Institute of Technology
Cambridge, Massachusetts 02139

Received April 17, 1979; revised September 13, 1979

Numerical calculations of diffusion processes in complex geometries in multi-dimensions is of current interest in many applications involving the solution of the coupled equations of radiation transport or thermal conduction, as well as in applications involving unstable hydrodynamic flows. The application of pseudospectral techniques to the implicit solution of the diffusion equation in a distorted two-dimensional grid for both linear and nonlinear problems is considered. The implicit pseudospectral equations on an $m \times n$ mesh result in a full $P \times P$ matrix ($P = (nm)^2$) which can be inverted by the methods we introduce. The examples given illustrate the success of pseudospectral techniques applied to the solution of these problems. The computational and memory requirements for machine implementation of pseudospectral techniques for a given accuracy are shown to be superior to those of standard finite difference technique. Coordinate transformations and interface patching techniques of interest in mixed Eulerian–Lagrangian modeling are illustrated in several examples.

1. INTRODUCTION

Numerical calculations of diffusion processes in problems of compressible hydrodynamics as well as simulations involving the solution of the coupled equations of hydrodynamics and radiation transport or thermal conduction [1–5] are central to present modeling efforts in inertial confinement fusion [6, 7] and other applications that may involve unstable hydrodynamic flows [8, 10]. Since pseudospectral techniques achieve high spatial resolution with increased economy compared to finite difference methods [11–14] it is natural to consider pseudospectral methods for these applications.

Because characteristic explicit diffusion times for the processes involved in the above applications are often several orders of magnitude smaller than the explicit time step allowed by the associated supersonic hydrodynamic flow, the diffusion equations should be solved implicitly [15]. The difficulty in applying pseudospectral

0021-9991/80/100093–20$02.00/0

techniques to these problems is that the matrix operator associated with the diffusion equation is full so the computational cost would be prohibitive if it were necessary to invert (or even store) the operator in multi-dimensional calculations. Fortunately, there is a procedure which allows us to solve the required spectral equations efficiently without either inverting or storing the operator [16]. Here we illustrate the technique for the solution of the heat equation on a highly distorted grid in two dimensions which is similar to grids encountered in many two-dimensional Lagrangian calculations for problems of current interest [17]. In addition, we analyze the accuracy of finite difference methods for these problems. In Cartesian geometry, we apply an ICCG technique [17] to invert the finite difference approximation to the spectral operator and compare the amount of additional work required to invert the spectral operator for the diffusion equation. We have also successfully used splitting techniques to solve these problems.

2. Heat Diffusion on a Distorted Grid

Consider the problem of solving the diffusion equation

$$c_v \frac{\partial U}{\partial t} = \nabla \cdot (K(x, z, t) \nabla U) \tag{1}$$

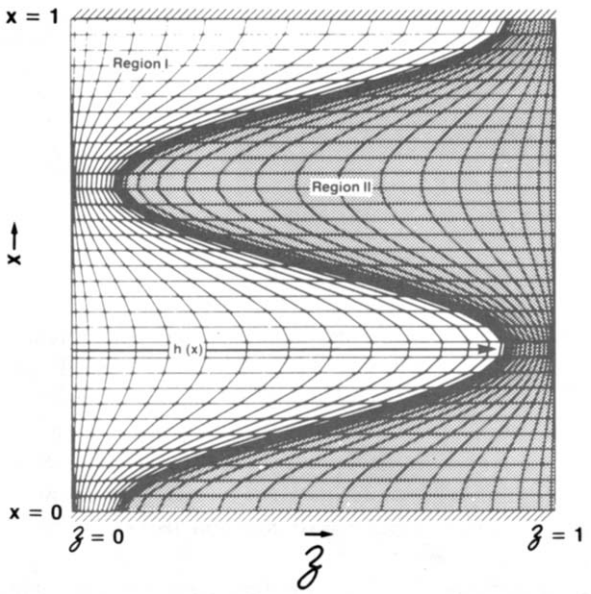

FIG. 1. Example of a distorted mesh. For the heat flow equation, along $x = 0$ and $x = 1$ there are insulating boundaries. The temperatures along the left and right boundaries ($z = 0$ and $z = 1$, respectively) are fixed and have the values $T_L = 10^3$ and $T_R = 10^{-2}$. The grid is distorted by a function $h(x)$ between the two regions, as indicated.

on the mesh illustrated in Fig. 1. The material between the boundaries at $z = 0$, $z = 1$ is uniform and initially cold, so $U(x, z, 0) = 0$. The top and bottom boundaries along $x = 0$, $x = 1$ are insulating while the temperature along the left and right boundaries, $z = 0$ and $z = 1$, are presumed fixed and have the values T_L and T_R, respectively. The distortion in the grid is caused by a stretching function $h(x)$, measured from the left boundary to the interface, as illustrated in Fig. 1. In this example, the "interface" between the two regions is artificial in the sense that the materials on either side are presumed homogeneous and identical to one another. This problem was first suggested by Kershaw [18] in his investigation of the accurate finite differencing of the diffusion equation on a Lagrangian mesh [19].

In many applications of interest, the interface is a real one between different inhomogeneous materials, and the severe distortion illustrated could result from the unstable hydrodynamic flow history of a given calculation. Such unstable flow, for example, can result from the nonlinear growth of a Rayleigh–Taylor instability at the ablation surface of a laser-driven pellet [8, 9].

In such highly distorted situations, there are ambiguities in the finite difference approximation to the diffusion operator which have been discussed by Kershaw [19]. In the present application, we have chosen to eliminate some of the difficulties associated with the "corner" terms, i.e., those terms which appear due to the nonorthogonal structure of the mesh, by mapping the mesh onto one which is orthogonal. Such an approach could find a variety of applications in mixed Eulerian–Lagrangian codes, for example [20–23].

The mapping used here is a simple coordinate stretching which is appropriate when $h(x)$ is single valued so regions I and II as illustrated in the figure form a star-shaped domain as viewed along $z = 0$ or $z = 1$. In more highly distorted flows, such a coordinate stretching cannot be applied and one would be forced to use more sophisticated mappings such as general Lagrangian transformations or conformal mappings [24, 25]. In the two latter cases, the procedure is only slightly more involved and does not preclude the application of the pseudospectral techniques that we describe below. The use of the coordinate stretching here serves mainly to illustrate our pseudospectral techniques for nontrivial examples. In addition, the nature of the "corner" terms is transparent in this approach as we demonstrate below. The "corner" terms are much more difficult to visualize in the general Lagrangian case [19].

A coordinate stretching appropriate to the geometry of Fig. 1 is

$$Z = 2\frac{z}{h(x)} - 1, \qquad -1 \leqslant Z \leqslant 1; \qquad \text{region I,} \tag{2}$$

$$\hat{Z} = 2\frac{z - h(x)}{1 - h(x)} - 1, \qquad -1 \leqslant \hat{Z} \leqslant 1; \qquad \text{region II.} \tag{3}$$

Equations (2) and (3) map both region I and region II onto rectangular regions in the (x, Z), and $(x, \hat{Z})$ coordinates, and the interface has the simple location $Z = 1$ (or $\hat{Z} = -1$). In the mapped coordinates, we have the relations

$$\left.\frac{\partial}{\partial x}\right|_z = \left.\frac{\partial}{\partial x}\right|_Z - (Z+1)\frac{h'}{h}\frac{\partial}{\partial Z}, \qquad \text{in region I,} \tag{4}$$

$$\frac{\partial}{\partial z} = \frac{2}{h}\frac{\partial}{\partial Z}, \tag{5}$$

and

$$\left.\frac{\partial}{\partial x}\right|_z = \left.\frac{\partial}{\partial x}\right|_{\hat{Z}} + \frac{h'}{1-h}(\hat{Z}-1)\frac{\partial}{\partial \hat{Z}}, \qquad \text{in region II,} \tag{6}$$

$$\frac{\partial}{\partial z} = \frac{2}{1-h}\frac{\partial}{\partial \hat{Z}}, \tag{7}$$

where $h = h(x)$ and $h' = dh(x)/dx$.

In addition, we require that the temperature field and the heat flux be continuous across the interface. The continuity of the heat flux requires that

$$\phi_{\mathrm{I,II}} = \frac{K}{(1+h'^2)^{1/2}}\left(-h'\frac{\partial U}{\partial x} + \frac{\partial U}{\partial z}\right)$$

be continuous along $z = h(x)$. In the mapped coordinates, the requirement is that

$$\phi_{\mathrm{I}} = \frac{K}{(1+h'^2)^{1/2}}\left(-h'\frac{\partial U}{\partial x} + \frac{h'^2}{h}(1+Z)\frac{\partial U}{\partial Z} + \frac{2}{h}\frac{\partial U}{\partial Z}\right)\Bigg|_{Z=1} \tag{8}$$

must be equal to

$$\phi_{\mathrm{II}} = \frac{K}{(1+h'^2)^{1/2}}\left(-h'\frac{\partial U}{\partial x} - \frac{h'^2}{1-h}(\hat{Z}-1)\frac{\partial U}{\partial \hat{Z}} + \frac{2}{1-h}\frac{\partial U}{\partial \hat{Z}}\right)\Bigg|_{\hat{Z}=-1}. \tag{9}$$

Similarly, the heat flow equation (1) becomes, in the mapped coordinates (x, Z),

$$\begin{aligned} c_v\frac{\partial U}{\partial t} = {} & \frac{\partial}{\partial x}\left(K\frac{\partial U}{\partial x}\right) - \frac{\partial}{\partial x}\left(\frac{h'}{h}K(1+Z)\frac{\partial U}{\partial Z}\right) \\ & - \frac{h'}{h}(1+Z)\frac{\partial}{\partial Z}\left(K\frac{\partial U}{\partial x}\right) \\ & + \frac{h'}{h}(1+Z)\frac{\partial}{\partial Z}\left(\frac{h'}{h}K(1+Z)\frac{\partial U}{\partial Z}\right) \\ & + \left(\frac{2}{h}\right)^2\frac{\partial}{\partial Z}\left(K\frac{\partial U}{\partial Z}\right) \end{aligned} \tag{10}$$

in region I. A similar expression holds in region II for $(x, \hat{Z})$. The "corner" terms which would appear in the distorted mesh operator appear as the cross-derivative

terms involving x and Z or x and $\hat{Z}$ in the mapped space. In formulating a finite difference approximation to equations such as (10) we have used a second-order accurate prescription which results in a nine-point finite difference operator approximation to the right-hand side of (10) for all interior points except at the interface. We usually apply one-sided derivative operators at the interface $Z = 1$, $\hat{Z} = -1$ to approximate the flux continuity relation $\phi_{\mathrm{I}} = \phi_{\mathrm{II}}$.

In two dimensions, the resulting discrete equations take the form

$$c_v \frac{\partial U_i}{\partial t} = M_{ik}^{\mathrm{FD}} U_k, \tag{11}$$

with implied summation of repeated indices. Here M_{ik}^{FD} is a $P \times P$ matrix where $P = (mn)^2$ and $m[n]$ is the number of points in the $x[z]$ direction and the subscripts, i, k, label the spatial gridpoints. The matrix M_{ik}^{FD} is a sparse matrix containing nine non-zero diagonals. Introducing δU by

$$U_i^{(n+1)} = U_i^{(n)} + \delta U_i, \tag{12}$$

where the subscript (n) denotes the nth time step, we obtain a discrete approximation to (11):

$$\left(\frac{c_v}{\delta t}\,\delta_{ik} - \alpha M_{ik}^{\mathrm{FD}}\right) \delta U_k = M_{ik}^{\mathrm{FD}}\, U_k^{(n)}. \tag{13}$$

Here δ_{ik} is the Kronecker delta, and $\alpha = 0$ corresponds to an explicit formulation of the diffusion equation while $\alpha = 1$ corresponds to a fully implicit formulation [15]. For unconditional stability in implicit calculations we should choose $\alpha \geqslant \frac{1}{2}$.

Many standard techniques exist for the numerical solution to the sparse matrix equation (13). In our particular examples, we use the general matrix ICCG algorithm of Kershaw [17] which has been demonstrated to handle successfully nine-diagonal problems of the sort we are discussing. We have also used an operator splitting technique which seems to work just as well in our examples.

Before introducing the pseudospectral treatment of the diffusion equation (1), we point out the importance of using an accurate finite difference operator approximation at the interface. Figure 2a illustrates a moderately distorted mesh which gives the steady state solution plotted in Fig. 2b. If $K(x, z, t) \equiv K$, a constant, the steady state solution is

$$U(x, z) = T_{\mathrm{L}} + (T_{\mathrm{R}} - T_{\mathrm{L}})z, \qquad 0 \leqslant z \leqslant 1, \tag{14}$$

so the isotherms are straight lines parallel to the x-axis. The curved isotherms in Fig. 2b are, in fact, principally due to the inaccuracy in treating the interface equation (8)–(9). The results plotted in Fig. 2b were obtained using first-order one-sided difference approximations to this equation. If one uses a higher order approximation (which, in this example, leads to a nine-point flux continuity equation), then the much

better results plotted in Fig. 2c are obtained. This example illustrates the importance of a careful finite difference formulation of the diffusion equation in distorted coordinates. We illustrate below that the finite difference operator we use to stabilize a pseudospectral scheme need not be chosen with such extensive care to obtain an accurate solution.

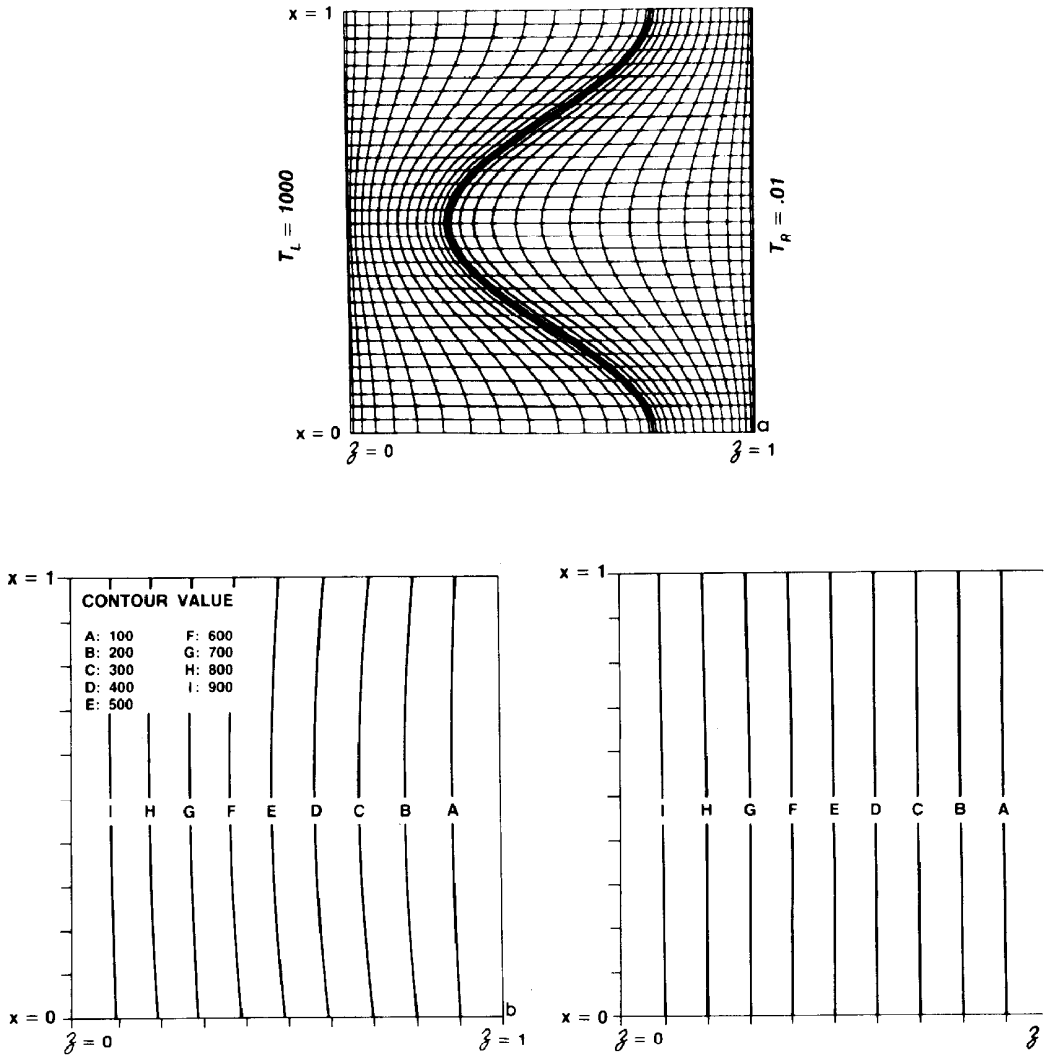

FIG. 2. (a) A moderately distorted mesh used in the problem whose steady state temperature contours are discussed in the text as illustrated in (b), which uses the low-order interface differenching discussed near the end of Section 2, and (c) the steady state finite difference solution when the more accurate nine-point formulation of the flux continuity equation at the interface is used.

3. Spectral Approximation to Heat Diffusion on a Distorted Grid

We now consider the pseudospectral formulation of Eq. (1). Because zero gradient conditions are imposed along the top and bottom, we expand in a Fourier cosine series in x. The fixed temperature boundary conditions at $z = \pm 1$ are best handled by an expansion in Chebyshev polynomials in the mapped coordinates Z and $\hat{Z}$ [14]. Thus, we expand U in region I as

$$U(Z_j, X_k, t) = \sum_{m=0}^{M} \sum_{n=0}^{N} \hat{U}_{nm}(t)\, T_n(Z_j) \cos(\pi m X_k), \tag{15}$$

where the Z_j are the collocation points

$$Z_j = \cos \pi(N-j)/N \qquad (j = 0, 1, \ldots, N) \tag{16}$$

and the collocation points X_k are

$$X_k = k/M, \qquad k = 0, 1, \ldots, M. \tag{17}$$

Here T_n is the Chebyshev polynomial of order n defined by $T_n(\cos\theta) = \cos(n\theta)$. The collocation points Z_j and X_k are chosen so that the double expansion (15) is efficiently computable using the fast Fourier transform (FFT) in order $O(MN \log NM)$ operations [14]. Of course, in region II, an expansion such as (15) is assumed in $\hat{Z}$ and x.

In order to calculate the x and Z derivatives in the mapped coordinates as required by (4) through (7), we take advantage of simple relations which relate the spectral coefficients of the derivative of a function to the spectral coefficients which represent the function. For finite Fourier series, if

$$f(x) = \sum \hat{f} e^{ikx}$$

then

$$f' = \sum ik\hat{f} e^{ikx}.$$

Similarly, if

$$g(Z) = \sum_{n=0}^{N} \hat{g}_n T_n(Z) \tag{18}$$

then

$$g'(Z) = \sum_{n=0}^{N} \hat{g}'_n T_n(Z), \tag{19}$$

where [14]

$$\hat{g}'_n = 2S_n/c_n. \tag{20}$$

Here $c_0 = 2$, $c_n = 0$ $(n < 0)$, $c_n = 1$ $(n > 0)$, and S_n satisfies the recurrence relation

$$S_n = S_{n+2} + (n+1)\hat{g}_{n+1}, \qquad 0 \leqslant n \leqslant N-1, \tag{21}$$

with $S_n = 0$ for $n \geqslant N$.

Substituting expansions (15) into (1) and using the derivative relations give the spectral matrix equation

$$\left(\frac{c_v}{\delta t}\,\delta_{ik} - \alpha M_{ik}^{\mathrm{sp}}\right)\delta U_k = M_{ik}^{\mathrm{sp}} U_k^{(n)}. \tag{22}$$

However, in contrast to (13), M_{ik}^{sp} is a full matrix which, for problems of interest (for example, $m = n = 100$ involves 10^8 elements), one cannot store, much less invert directly.

We have discovered [16, 25] a fast, efficient iterative procedure for solving (22) in which the full matrix M^{sp} need never be evaluated or stored! The method allows solution of (22) with little more work than is necessary to solve (13) with the same number of grid points as spectral modes. Here we briefly outline the method.

Consider the formal equation

$$LU = F, \tag{23}$$

where L is a differential operator. Suppose that the spectral approximation to the equation is written $L_{\mathrm{sp}} U_{\mathrm{sp}} = F_{\mathrm{sp}}$. The key idea is that we can construct an operator L_{ap} that approximates L_{sp} in the sense that

$$\|L_{\mathrm{sp}}^{-1} L_{\mathrm{ap}}\| = O(1) \qquad \text{and} \qquad \|L_{\mathrm{ap}}^{-1} L_{\mathrm{sp}}\| = O(1) \quad \text{as } P \to \infty, \tag{24}$$

where P is the total number of modes and such that L_{ap} has a sparse matrix representation so it requires only $O(P)$ storage and such that L_{ap} is at least as efficiently invertible as low-order finite difference approximations to (23).

It is remarkable that we can construct such approximations L_{ap} to the spectral operators L_{sp} that satisfy all the above restrictions as well as

$$\|L_{\mathrm{ap}}^{-1} L_{\mathrm{sp}}\| \lesssim 2.5, \qquad \|L_{\mathrm{sp}}^{-1} L_{\mathrm{ap}}\| \lesssim 1 \tag{25}$$

for nearly arbitrary operators L and all resolutions P. While the detailed construction of L_{ap} is given elsewhere [16, 26], here we mention that for the current thermal diffusion problems L_{ap} is simply the lowest-order finite difference operator on the collocation grid Z_j, X_k.

Once L_{ap} is constructed, various iteration schems [16, 26] can be used to achieve machine accuracy in a bounded number of iterations, independent of the resolution P.

For example, conjugate gradient iterations to solve (22) give a factor 10^7 improvement in accuracy after only six iterations, with the convergence improving slightly as P increases!

The simplest way to use this approximate spectral operator calculus is to replace (22) by the scheme

$$\left(\frac{c_v}{\delta t}\delta_{ik} - 2.5\, M_{ik}^{\mathrm{FD}}\right)\delta U_k = \left(M_{ik}^{\mathrm{sp}} - 2.5\, M_{ik}^{\mathrm{FD}}\right)\, U_k^{(n)}. \tag{26}$$

Since (25) holds, this scheme is unconditionally stable. Since M^{FD} is sparse, (26) can be solved efficiently and stored compactly.

In the two-dimensional examples given below, we invert the matrix on the left-hand side of (26) using the general nine-diagonal ICCG scheme of Kershaw [17], and the right-hand side is easily evaluated using the fast Fourier transform. It is of interest that the finite difference operator M_{ik}^{FD} need not be as carefully formulated as that required to obtain the solution of Fig. 2c. Using the finite difference operator used in the example of Fig. 2b in (26), the spectral solution obtained is plotted in Fig. 3. The only requirement of the finite difference operator M^{FD} is that it should have a reasonable approximation to the spectrum of the spectral operator in order to stabilize the scheme (26). Thus, one need not take as much care in constructing an accurate finite difference operator (see, for example, Ref. [19]) in order to stabilize the spectral scheme. Scheme (26), when stabilized, results in a solution which retains the full spectral accuracy except for time stepping errors. Recent advances [27] in the development of high-order accurate splitting methods can be used to reduce the time stepping errors.

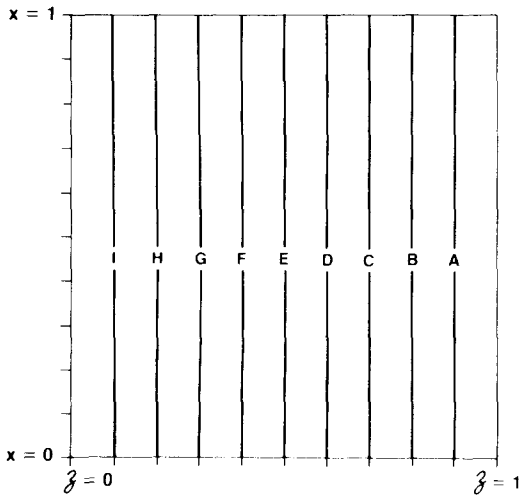

FIG. 3. Spectral solution for the diffusion equation using the finite difference operator used in Fig. 2b.

4. Accuracy

In order to study the accuracy of spectral methods for diffusion problems with interfaces, we consider the simple one-dimensional model problem

$$\frac{\partial u}{\partial t} = \frac{\partial^2 u}{\partial x^2} \qquad (-2 \leqslant x \leqslant 0), \tag{27}$$

$$\frac{\partial v}{\partial t} = \frac{\partial^2 v}{\partial x^2} \qquad (0 \leqslant x \leqslant 2) \tag{28}$$

with the boundary conditions

$$u(-2, t) = v(+2, t) = 0 \tag{29}$$

and the continuity conditions

$$u(0, t) = v(0, t), \tag{30}$$

$$\frac{\partial u}{\partial x}(0, t) = \frac{\partial v}{\partial x}(0, t) \tag{31}$$

applied at the "interface" $x = 0$. Of course, the interface at $x = 0$ in (27)–(31) satisfies the heat equation with diffusion coefficient 1 on $-2 \leqslant x \leqslant 2$.

To solve (27)–(31) spectrally we employ the Chebyshev expansions

$$u(x, t) = \sum_{n=0}^{N} a_n T_n(x - 1), \tag{32}$$

$$v(x, t) = \sum_{m=0}^{M} b_n T_n(x + 1). \tag{33}$$

The resulting spectral equations are of the form

$$\frac{\partial}{\partial t}\begin{pmatrix} u \\ v \end{pmatrix} = L_{\text{sp}}\begin{pmatrix} u \\ v \end{pmatrix}. \tag{34}$$

In the notation of Section 3, L_{ap} will be a finite difference approximation to (27)–(31) on the associated collocation grid of $N + M + 1$ points (including boundary and interface points).

A good way to study the error in the spectral approximation (34) is to find the

system (27)–(31) are

$$u(x, t) = v(x, t) = \sin[|\lambda|^{1/2}(x + 2)]e^{\lambda t}, \tag{35}$$

TABLE I

Accuracy of Pseudospectral Approximation to the Diffusion Equation with an Interface

	Spectral cutoff $N = M$		
	5	10	20
	Number of interior collocation points		
	9	19	39
Absolute error in spectral approximation to the eigenvalue $\lambda = -(k\pi/4)^2$			
$k = 1$	9×10^{-5}	$<10^{-10}$	$<10^{-10}$
$k = 2$	6×10^{-4}	3×10^{-8}	$<10^{-10}$
$k = 3$	2×10^{-3}	5×10^{-6}	$<10^{-10}$
$k = 10$	—	9×10^{-1}	2×10^{-6}
$k = 20$	—	—	2×10^{-1}
Absolute error in finite difference approximations to the eigenvalue $\lambda = -(k\pi/4)^2$			
$k = 1$	5×10^{-2}	1×10^{-2}	3×10^{-3}
$k = 2$	1×10^{-2}	3×10^{-3}	7×10^{-4}
$k = 3$	2×10^{-1}	4×10^{-2}	8×10^{-3}
$k = 5$	—	—	2×10^{-1}
Spectral norms			
$L_{ap}^{-1} L_{sp}$	1.910	2.202	2.340
$L_{sp}^{-1} L_{ap}$	0.873	0.967	0.992

where the eigenvalues λ are

$$\lambda = (k\pi/4)^2 \tag{36}$$

for $k = 1, 2, 3, \ldots$.

The errors in the finite difference and pseudospectral approximations to this problem are listed in Table I for various k, N, M. The spectral norms of $L_{ap}^{-1} L_{sp}$ and $L_{sp}^{-1} L_{ap}$ are also given to show that the method introduced in Section 3 for solving the spectral equations works. Observe the extremely rapid convergence of the spectral results compared to the finite difference results.

5. Applications of Spectral Methods to Heat Diffusion Problems

In this section we give examples of solutions of (1)–(9) using a variety of mesh sizes for two different linear problems: (i) a moderately distored mesh where $k(x) = 0.25 + 0.25 \cos 2\pi x$ (a 3 to 1 stretching); and (ii) a highly distorted mesh ($8\frac{1}{2}$ to 1 stretching) with sharp corners, like that discussed by Kershaw [18]. The meshes are illustrated in Fig. 2a and Fig. 4.

In order to evaluate the amount of extra difficulty in converging to a solution of the implicit equations of a given required accuracy (10^{-7} was used as an error criterion in these examples according to the procedure suggested in Ref. [17]), Table II compares the number of ICCG iterations required for meshes of various sizes for both "large" and "small" time steps for the grid of Fig. 2a. In Table II, $\Delta t_{\exp}$ is the time step necessary for stability of an explicit first-order Euler time integration of the spectral equations. The dimensional time τ used to measure the step size is C_v/K. The time required for the transient solution to die out is roughly $\pi^2 K/C_v$, as can be easily seen from the exact time-dependent solution to the problem

$$U(x, z, t) = T_L + (T_R - T_L)z + \sum_{n=1}^{\infty} \hat{u}_n \sin n\pi x \, e^{-n^2\pi^2 t/\tau}, \tag{37}$$

where

$$\hat{u}_n = \frac{2}{n\pi}(T_R \cos \pi n - T_L).$$

Table II shows that there is little difference in the amount of work required to achieve

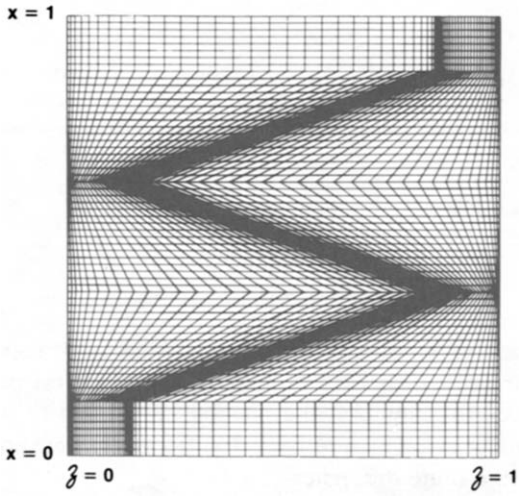

FIG. 4. A highly distorted mesh ($8\frac{1}{2}$: 1 coordinate stretching) with sharp corners such as that considered in Ref. [18].

TABLE II

Grid size	Time step $\Delta t/\tau$	$\Delta t/\Delta t_{exp}$	Number of ICCG iterations	
			Finite difference	Spectral
32×32	0.003	3×10^3	14	22
16×16	0.003	2×10^2	8	11
8×8	0.003	10	9	10
32×32	0.03	3×10^4	38	41
16×16	0.03	2×10^3	16	18

the same relative accuracy for the spectral procedure as that required for the finite difference solution with the same number of spatial mesh points as spectral modes. Since the spectral results are much more accurate than the finite difference results on the same grid, it appears that pseudospectral methods enjoy the same relative advantage in computing economy in situations involving the implicit solution of the diffusion equations as they do in explicit solutions of the Navier–Stokes equations [11]. Most of the computing time of the present calculations is spent in the ICCG iterations and most of the storage also goes to the ICCG scheme. The evaluation of $M^{sp}U$ is hidden in these large overhead operations so the computer time is nearly proportional to the number of ICCG iterations.

Figure 5 compares the time-dependent behavior of the numerical solution to the

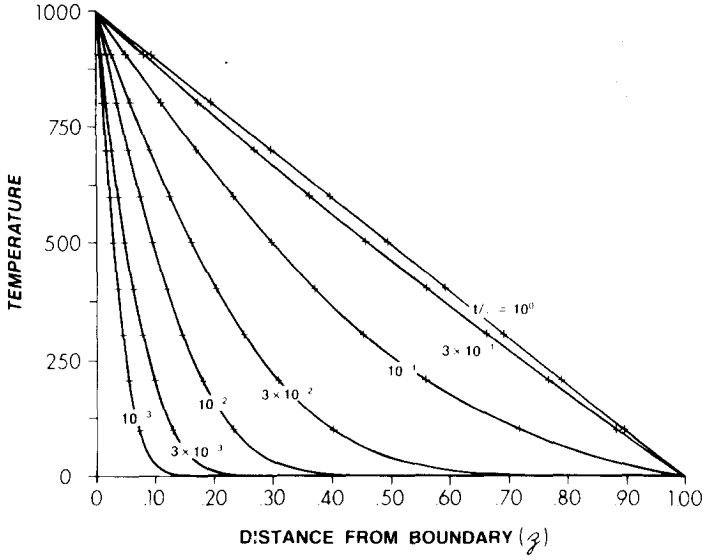

FIG. 5. Time-dependent exact solution for the linear heat flow problem compared to the numerically obtained time-dependent spectral solution for the distorted mesh illustrated in Fig. 1. The plotted points represent the results obtained numerically from the spectral code.

problem compared to the exact solution (37) for a severe distortion (a 9 : 1 stretching of the form $h(x) = 0.5 + 0.4 \cos 3\pi x$) illustrated in Fig. 1 for the linear problems for the 32×32 mesh. The 16×16 spectral solutions were essentially the same as the 8×8 spectral solutions for the time-independent steady state. The time-dependent solutions converge rapidly as the number of spectral modes increases.

In addition to the highly distorted cosine mesh discussed above, we have also obtained solutions to a highly distorted ($8\frac{1}{2} : 1$ distortion) grid with sharp corners, similar to that discussed by Kershaw in Ref. [18], illustrated in Fig. 4 for a 64×64 mesh. The time steps for this example are intermediate between those given in Table II and represent the time for the front of a thermal wave to travel approximately 1/10th of the entire mesh distance in the z-direction and corresponds to a "large" time step in most practical problems of interest, and in fact is of order 2×10^5 times the explicit time step required by a first-order Euler time integration scheme (see Table III) for the 64×64 point example. In the example given, the time step would be larger than that required for a sound wave to cross the smallest zone (which is the least restrictive time step restriction on most design codes in use in inertial fusion target design calculations). The results are summarized in Table III.

The large number of iterations required in both the case of finite differences and the spectral scheme is due to the nature of the nine-diagonal ICCG procedure for a general matrix. If one takes advantage of the relative economy of the ICCG procedure for a symmetric matrix (as in Ref. [18]), the number of iterations can be significantly reduced (perhaps by a factor of 2 or 3). The major difficulty with the general procedure is that the condition number ($|\lambda_{\max}/\lambda_{\min}|$) of the matrix operator is *squared* in the unsymmetric matrix ICCG procedure discussed in Ref. [17].

The interesting conclusion from our runs is that the spectral "overhead" for equal numbers of spatial mesh points and spectral modes is relatively minimal. The major portion of the work is involved in the LU decomposition of the matrix operator, and the absolute accuracy advantage gained for the spectral overhead is justified. The finite difference operator used to construct Table III was the more accurate (nine-diagonal) operator introduced in Section 2 in the discussion of Fig. 2c. Both the finite difference results and the spectral results exhibit "sharp corner" errors in the contours whose size is roughly that of the mesh spacing near these contours (see Fig. 6 and 7). The spectral results plotted in Fig. 7 have approximately the same accuracy on a

TABLE III

Grid size	Time step $\Delta t/\tau$	$\Delta t/\Delta t_{\exp}$	Number of ICCG iterations: Finite difference	Number of ICCG iterations: Spectral
64×64	0.01	1.7×10^5	74	100
32×32	0.01	10^4	24	30
16×16	0.01	7×10^2	13	14

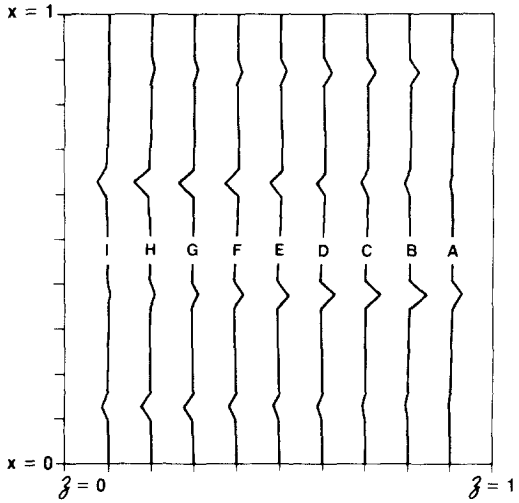

FIG. 6. Finite difference solution for a 32×32 grid (such as that illustrated for a 64×64 grid in Fig. 4).

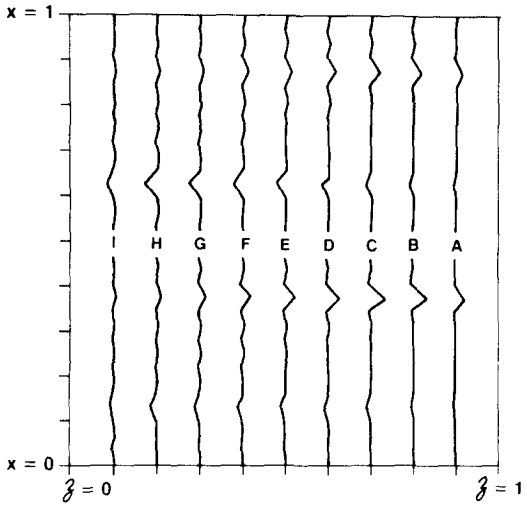

FIG. 7. Spectral solution for a 32×32 grid (such as that illustrated for a 64×64 grid in Fig. 4).

32×32 point mesh (except at the "corners") as that obtained in Ref. [18], which used a 75×75 point mesh. This result is consistent with the accuracy difference between the finite difference and spectral approximations illustrated in Table I. The spectral solution to the same problem on a 64×64 mesh is plotted in Fig. 8. These examples are a severe test of the spectral method because of the discontinuities (sharp

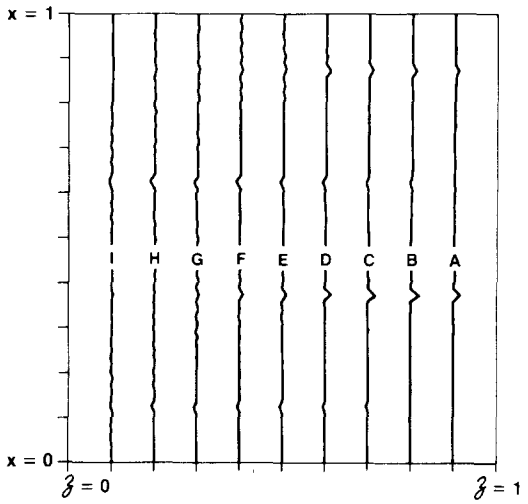

FIG. 8. Spectral solution for a 64 × 64 grid with sharp corners (see Fig. 4). Note the improved accuracy (see Fig. 7) due to the added resolution.

corners) in the interface. For similar problems where the corners have been smoothed, one cannot distinguish the difference from the plots in the results between the 32 × 32 and 64 × 64 spectral results.

In addition to the examples given for the linear thermal conduction problem, we have applied scheme (26) to a nonlinear problem in which K in (1) is given by $K = K_0(T/T_L)^{5/2}$. The problem is to solve for the propagation of a nonlinear thermal wave similar to the one that can propagate in a plasma with electron conduction, a problem of considerable interest in inertial confinement studies. The solution is approximately self-similar [29] until the wave front reaches the $z = 1$ boundary. The solution to Eq. (1) in the infinite domain $0 \leqslant z \leqslant \infty$ for the nonlinear problem can be written in the form [29] $T(z) = T_L f(\xi)$, where $\xi = z/(K_0/C_v)t)^{1/2}$ and $f(\xi)$ is obtained by solving the resulting second-order ordinary differential equation with the boundary conditions $f(0) = 1$, $f(\infty) = 0$. The position of the front of the nonlinear wave (defined by $\partial T/\partial Z = \infty$) as a function of time is given by

$$z_f \sim \left(\frac{K_0}{c_v} t\right)^{1/2}. \tag{38}$$

Figure 9 illustrates the time-dependent evolution of the isotherms which propagate along z obtained for a 32 × 32 grid, illustrated in Fig. 10a. In terms of the dimensionless time t/τ ($\tau = c_v/K_0$), the curves in Fig. 9 were obtained by plotting $T(\bar{z})$, where $\bar{z}$ is obtained by averaging over the (nearly constant) values of the z coordinate of an isotherm for a fixed value of t/τ. The values of t/τ for the six curves of Fig. 9 were $t/\tau = 0.23$, 0.38, 0.58, 0.78, 1.03, and 1.48, where the smallest value of t/τ is represented by the leftmost curve. For values of t/τ greater than about 1.5, the solu-

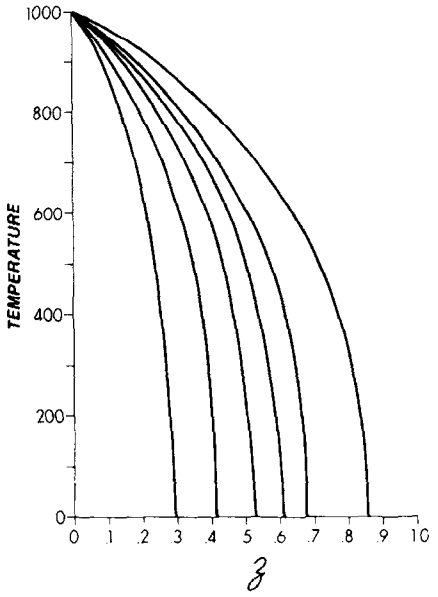

FIG. 9. Time-dependent temperature profiles for the nonlinear thermal conduction problem on the mesh of Fig. 10a. The z-coordinate for each of the indicated temperature values on the isotherms labeled A–I (see Fig. 10b) was obtained by averaging the z values across each contour. The profiles illustrated were obtained at the dimensionless times $t/\tau = 0.23$, 0.38, 0.58, 0.78, 1.03, and 1.48, where the value of t/τ for each curve increases from left to right in the figure.

tion can no longer be considered self-similar. The position of the front as a function of time for the given values of t/τ was found to be

$$\bar{z}_f \sim t^{0.502 \pm 0.002}, \tag{39}$$

in agreement with the time behavior of Eq. (38). The "exact" isotherms representing the spatial behavior of the solution should be straight lines and the numerically obtained spectral solution at a late time, just before the thermal wave reaches the $x = 1$ boundary is illustrated in Fig. 10b. This problem is illustrative of a difficult nonlinear problem in that the thermal conductivity changes by 13 orders of magnitude across the grid. The time step used for this problem ($\Delta t/\tau \sim 5 \times 10^{-3}$) corresponds to the approximate time step restrictions which would be required in a problem with the heat flow coupled to supersonic hydrodynamic flow, where the front of the thermal wave can propagate only a few grid zones per time step. The time step used is approximately 5000 times the explicit time step allowed by an explicit formulation ($\alpha = 0$ in (26)). The number of ICCG iterations required for the same relative error (10^{-7}) for this particular problem was 12.

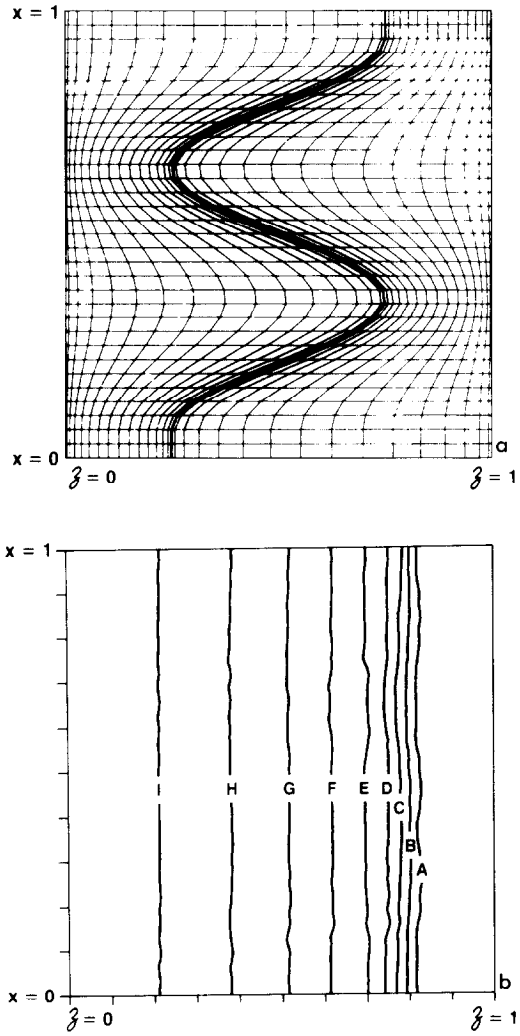

FIG. 10. (a) A 32×32 distorted mesh for the nonlinear conduction problem. (b) The contours at a late time in the calculation before the nonlinear wave front reaches the $z = 1$ boundary.

6. CONCLUSIONS

The above examples demonstrate that pseudospectral techniques can be successfully employed in the solution of implicit diffusion equations of interest in many current applications. The computational efficiency and memory requirements of the pseudospectral techniques for a given accuracy exceed those of more standard finite difference techniques (see Table I). Although we have restricted the discussion in this

paper, for the two-dimensional problems, to a comparison of finite difference methods with spectral methods to the case of incomplete conjugate gradient iterations, we remark that essentially identical results are obtained in those cases where other iterative schemes are used. In Ref. [16], an implicit alternating direction (ADI) method was used by one of us in solving the heat equation with Dirichlet boundary conditions in a highly distorted domain in cylindrical geometry. The only additional overhead incurred computationally in the solution to Eq. (26) when ADI methods are used is the evaluation of the $M_{ik}^{sp} U^{(n)}$ term. Compared to the total computational work per iteration, the computational work involved in evaluating the term is not significant because of the enhancements in speed and efficiency due to the fast transforms used in computing the spectral operator.

The use of coordinate transformations and interface patching allows spectral methods to be applied in complicated geometries using mixed Eulerian–Lagrangian formulations such as those given in Refs. [21–23]. We have shown that first-order-accurate representation of the finite difference approximate operator both stabilizes the spectral scheme (as in Eq. (26)) and gives accurate spectral solutions.

The methods introduced here remove the barriers to the successful application of the high-spatial-accuracy pseudospectral techniques to combined hydrodynamic/diffusion problems. The methods introduced are as efficient, storage-wise and computationally, as present finite difference approaches.

The high resolution capabilities of pseudospectral techniques to resolve phenomena near material interfaces should give these schemes a significant advantage over a finite difference methods in many applications of interest.

ACKNOWLEDGMENT

The major support for this work was provided by the Theoretical and Theoretical Design Divisions of the Los Alamos Scientific Laboratory of the University of California under contract to the United States Department of Energy. In addition, one of the authors (R.L.M.) acknowledges additional partial support from the Laboratory for Laser Energetics at the University of Rochester under the Laser Fusion Feasibility Project sponsored by Exxon Research and Engineering Company, Northeast Utilities Company, General Electric Company, Empire State Electric Research Corporation, and the New York Energy Research and Development Administration. Additional partial support to one author (S.A.O.) from the office of Naval Research under Contract N00014-77-C-0138 is gratefully acknowledged.

REFERENCES

1. G. B. ZIMMERMAN, "Numerical Simulation of the High Density Approach to Laser Fusion," Lawrence Livermore Laboratory, Report UCRL-74811 (1973).
2. H. D. SHAY, "Lasnex Simulation of X-Ray Generation," Lawrence Livermore Laboratory, Report UCID-16297 (1973).
3. R. C. ANDERSON AND M. T. SANFORD II, "Yokifer: A Two-Dimensional Hydrodynamics and Radiation Transport Program," Los Alamos Scientific Laboratory, Report LA-5704-MS (1975).

4. S. L. THOMPSON, "CSQ11—An Eulerian Finite Difference Program for Two-Material Response," Pt. 1, Sandia Laboratories Report SAND77-1339 (1979).
5. D. G. COLOMBANT *et al.*, *Phys. Fluids* **18** (1975), 1687.
6. G. S. FRALEY *et al.*, *Phys. Fluids* **17** (1974), 474.
7. K. A. BRUECKNER AND S. JORNA, *Rev. Mod. Phys.* **46** (1974), 2.
8. D. B. HENDERSON, R. L. MCCRORY, AND R. L. MORSE, *Phys. Rev. Lett.* **33** (1974), 205.
9. G. S. FRALEY *et al.*, Explosion, stability, and burn of multi-shell fusion pellets, *in* "Proceedings, Fifth International Conference on Plasma Physics and Controlled Nuclear Fusion Research, IAEA, 1975," Vol. II, p. 543.
10. R. L. MCCRORY, R. L. MORSE, AND K. A. TAGGART, *Nucl. Sci. Eng.* **64** (1977), 163.
11. S. A. ORSZAG, *J. Fluid Mech* **49** (1971), 75.
12. S. A. ORSZAG, *Monthly Weather Rev.* **102** (1974), 1.
13. H. WENGLE AND J. H. SEINFELD, *J. Comput. Phys.* **26** (1978), 87.
14. D. GOTTLIEB AND S. A. ORSZAG, "Numerical Analysis of Spectral Methods," SIAM Regional Conference Series in Applied Mathematics, SIAM, Philadelphia, 1977.
15. R. D. RICHTMYER AND K. W. MORTON, "Difference Methods for Initial Value Problems," Interscience, New York, 1967.
16. S. A. ORSZAG, *J. Comput. Phys.* **37** (1980), 70.
17. D. S. KERSHAW, *J. Comput. Phys.* **26** (1978), 43.
18. D. S. KERSHAW, *in* "Laser Program Annual Report—1976," pp. 4–52, Lawrence Livermore Laboratories Report UCRL-50021-76 (1978).
19. D. S. KERSHAW, "Differencing of the Diffusion Equation in LASNEX," Lawrence Livermore Laboratory Report UCID-17424 (1977).
20. F. H. HARLOW AND A. A. AMSDEN, *J. Comput. Phys.* **16** (1974).
21. R. S. CRAXTON AND R. L. MCCRORY, *J. Comput. Phys.* **33** (1979), 432.
22. D. V. ANDERSON, *J. Comput. Phys.* **17** (1975), 246.
23. T. P. BORIS AND D. L. BOOK, *J. Comput. Phys.* **20** (1976), 397, and references therein.
24. R. MENIKOFF AND CHARLES ZEMACH, "Methods for Numerical Conformal Mapping," Los Alamos Scientific Laboratory, Report LA-7836-MS (1979).
25. S. A. ORSZAG AND R. L. MCCRORY, Cambridge Hydrodynamics, Incorporated Memorandum No. 7901 to The Thoretical and Theoretical Design Divisions of the Los Alamos Scientific Laboratory (1979), (unpublished).
26. S. A. ORSZAG, to be published.
27. S. A. ORSZAG AND M. DEVILLE, to be published.
28. L. SPITZER, "Physics of Fully Ionized Gases," 2nd ed., Interscience, New York, 1962.
29. YA. B. ZEL'DOVICH AND YU. P. RAIZER, "Physics of Shock Waves and Temperature Hydrodynamic Phenomena," Vol. II, pp. 672 ff., Academic Press, New York, 1967.